An International Journal of Optimization and Control: Theories & Applications
ISSN: 2146-0957 eISSN: 2146-5703
Vol.16, No.2, pp.717-731 (2026)
https://doi.org/10.36922/IJOCTA025510233

RESEARCH ARTICLE

Various solutions of (2+1)-dimensional sixth-order breaking soliton systems using bilinear neural network method

Nguyen Minh Tuan†, Nguyen Hong Son†, and Huynh Trong Thua*

Department of Computer Science, Faculty of Information Technology, Posts and Telecommunications Institute of Technology City, 11 Nguyen Dinh Chieu, Sai Gon ward, Ho Chi Minh city, Viet Nam
minhtuan@ptit.edu.vn, songngh@ptit.edu.vn, thuaht@ptit.edu.vn

ARTICLE INFO

Article History:
Received: December 17, 2025
Revised: January 24, 2026
Accepted: February 10, 2026
Published Online: March 30, 2026

Keywords:
Breaking soliton system
Bilinear neural network method (BNNM)
Softmax method
High-order soliton equations
Solitary wave solutions
Analytic exact solution

AMS Classification 2010:
26A33; 34A08; 35H15; 34K50 47H10; 60H10

ABSTRACT

This paper firstly introduces the (2+1)-dimensional sixth-order breaking soliton system (SBSS) using the bilinear neural network method, providing many types of solutions. A new structure of the SBSS is investigated, and new solutions are gathered. The solutions are expressed in terms of basic activation functions and are derived by applying these activation functions. Using the Hirota bilinear operator, the original nonlinear partial differential equation is reduced to a more tractable form. The bilinear neural network approach yields various classes of solutions, including kink, rogue, peak, breather, lump-type, and spike-type solutions. These solutions are expressed in terms of elementary functions, revealing the various dynamical behaviors inherent in the system. The results obtained not only generalize known solutions but also illustrate a deeper insight into the complex wave propagation phenomena described by the sixth-order breaking soliton equation.

1. Introduction

The study of solitonic solutions to nonlinear differential equations, particularly breaking soliton systems, has attracted significant research attention. A variety of analytical techniques have been developed to investigate these solutions under different parameter regimes. For instance, the Tanh method has been widely applied to construct explicit solutions and examine their graphical behaviors. [1] Using non-isospectral Lax pairs, a novel (2+1)-dimensional breaking soliton equation was derived and integrated with lower-order solutions from the Kaup–Newell hierarchy. [2] Lie symmetry analysis has further provided closed-form and exact solutions to Bogoyavlenskii-type equations, uncovering diverse nonlinear wave structures, including singular, bell-shaped, breather-type, and kink waves. [3,4] Additionally, the extended homoclinic test approach and generalized variable separation method have facilitated the derivation of non-traveling wave solutions involving arbitrary functions. [5] In the context of fractional calculus, Jumarie's modified Riemann–Liouville derivative has been employed to obtain trigonometric, rational, and hyperbolic solutions for space–time fractional models. [6] Moreover, investigations into interaction dynamics revealed bright–dark solitary wave behaviors arising from the Boussinesq equation with dual dispersion

*Corresponding Author
†*These authors contributed equally to this work.*

and the (3+1)-dimensional modified Korteweg–de Vries–Kadomtsev–Petviashvili system. [7]

The generalized breaking soliton (gBS) equation, which models interactions between long and Riemann waves, has been extensively investigated using analytical and numerical techniques. Bell polynomials combined with Hirota's bilinear method provided explicit soliton solutions, [8] while homoclinic theory and numerical simulations revealed breather and rogue wave dynamics. [9] Several solution approaches, such as the (G'/G^2) expansion and F-expansion methods, have been employed to obtain soliton, kink, and periodic wave structures for fractional nonlinear partial differential equations (NPDEs). [10] The integrability of higher-dimensional forms, including the (2+1)-dimensional equations, was established using Hereman's method and Painlevé analysis. [11,12] A five-parameter gBS equation has been shown to encapsulate multiple classical soliton models as special cases, [13] while its (3+1)-dimensional extension generated multi-soliton and lump solutions through Hirota bilinear forms and generalized exp-function techniques[14–16]. Deeper symmetry structures have also been studied: connections between nonlocal and residual symmetries were revealed using Lax pairs, and Hirota's method enabled the construction of N-soliton solutions. [17] Furthermore, Lie symmetry methods combined with Noether's theorem were applied to classify symmetries and derive conservation laws. [18]

Beyond theory, experimental validation has been demonstrated through polarization tracking of vector soliton molecules using advanced fast polarimetry, highlighting the physical relevance of gBS models. Wronskian techniques and the tan-expansion method have been instrumental in constructing multi-soliton solutions and fractional extensions of nonlinear equations. [19–21] Certain $(2+1)$-dimensional models have been successfully reduced to $(1+1)$-dimensional forms, enabling the application of Darboux transformations, [22] with broad implications across fluid mechanics, plasma physics, and nonlinear optics. [23] He's variational principle and semi-inverse methods have further contributed by deriving new functionals and exact soliton solutions. [24] More advanced approaches including the Lie group method, homoclinic test technique, and three-wave method have provided breather and periodic solutions to complex nonlinear systems. [25,26] In addition, theta-function solutions have been achieved through the F-expansion method, [27] while symbolic computation and Hirota bilinearization have been effectively employed in the study of (2+1)-dimensional breaking soliton systems. [28,29] Building on these foundations, the present work applies the bilinear neural network method (BNNM) to obtain solutions of the breaking soliton system (BSS), formulated as follows, [30] in Equation 1:

$$u_{xt} - 2u_y u_{xx} - 4u_x u_{xy} - u_{xxxy} + p\left(u_x\right)^2 u_{tx} + q\left(u_{xx}u_{xxx} + u_x.u_{xxxx}\right) + r u_{xxxxxx} = 0 \qquad (1)$$

Recently, data-free numerical methods, such as bilinear neural networks and homotopy perturbation techniques, have been successfully applied to generate accurate breather, lump, and rogue wave solutions[31–35]. Physics-informed neural networks and their variants have further advanced the modeling of soliton dynamics in modified Korteweg–de Vries-type systems[36]. In parallel, classification frameworks based on mapping and variable separation have expanded the diversity of obtainable solutions, [37] while symbolic computation tools continue to provide automated procedures for soliton solution construction. [38] Moreover, modified bilinear approaches have facilitated the derivation of exact multi-soliton solutions without resonance effects. [39] To address the challenges of solving nonlinear differential equations, the BNNM has recently been deployed as a powerful hybrid strategy, capable of producing both analytical and numerical solutions. This approach serve as a bridge between traditional analytical techniques such as the Hirota bilinear method and the inverse scattering transform and modern data-driven methodologies in computational mathematics and artificial intelligence. In particular, BNNM exploits the structural properties of bilinear forms, which are central to many integrable systems, while embedding them within neural network architectures that can efficiently learn complex mappings between governing parameters and corresponding solution structures.

The BNNM framework typically begins by transforming the target NPDE into its bilinear form, often achieved through Hirota derivatives or Bell polynomials. [40,41] This bilinearization linearizes the nonlinear dynamics in a multiplicative sense, allowing the solution space to be expressed in terms of exponential, trigonometric, or rational functions. Within the neural network architecture, these bilinear operators are explicitly encoded, ensuring that the model intrinsically preserves the algebraic structure of the governing NPDE. [42] This structural embedding distinguishes BNNM from generic deep neural networks, which usually require extensive regularization or external constraints to guarantee physically meaningful solutions. [43]

A key advantage of BNNM is the ability to operate without explicit training data in certain configurations. [44] Instead, the method is inherently physics informed. The loss function of the encoder is constructed directly from the governing NPDE and the bilinear representation governing the NPDE. [45] The optimization process seeks to minimize the residual of the equation across collocation points, producing solutions that satisfy the governing dynamics up to a prescribed tolerance. [46] This strategy shares conceptual similarities with physics-informed neural networks but integrates problem-specific bilinear structures, thereby improving accuracy, stability, and convergence for soliton-type solutions. [47] Compared with traditional bilinear approaches, BNNM offers several significant enhancements. [48] First, BNNM effectively addresses high-dimensional systems including (3+1)-dimensional generalized breaking soliton equations without succumbing to the exponential growth in computational complexity typical of symbolic methods. [49] Second, BNNM is capable of approximating analytically challenging solutions, such as non-traveling waves, lump–rogue wave interactions, and multi-soliton collisions. Finally, BNNM demonstrates flexibility in handling systems with variable coefficients, nonlocal interactions, or fractional derivatives, where classical bilinear transformations are cumbersome or infeasible. [50]

2. Bilinear neural network method

Definition 1 (Hirota bilinear operator)**.** *The Hirota bilinear operator defined with the features of the D-operator is shown as follows[43]:*

$$D_t^m D_x^n f(t,x)\cdot g(t,x) = \left.\frac{\partial^m}{\partial s^m}\frac{\partial^n}{\partial y^n} f(t+s,x+y)\, g(t-s,x-y)\right|_{s=0,\,y=0}, \quad m,n=0,1,2,\cdots \tag{2}$$

Compared to the Leibniz rule, the differentiation of a product rule could be written as follows:

$$\frac{\partial^m}{\partial t^m}\frac{\partial^n}{\partial x^n} f(t,x)\cdot g(t,x) = \left.\frac{\partial^m}{\partial s^m}\frac{\partial^n}{\partial y^n} f(t+s,x+y)\, g(t+s,x+y)\right|_{s=0,\,y=0}, \quad m,n=0,1,2,\cdots \tag{3}$$

The BNNM is a hybrid framework based on neural network model shown in Figure 1 that combines classical bilinear techniques with modern neural architectures to solve NPDEs. The method proceeds through the following stages:

Step 1 (Bilinearization) : Given a general equation is shown as follows:

$$F\left(f, f_x, f_y, f_t, f_{xy}, f_{xt}, f_{yt}, f_{xyt}, \cdots\right) = 0 \tag{4}$$

where f_x, f_y, f_t, f_{xx}, f_{xt}, f_{yt}, $\cdots$ demonstrate the derivative respect to x, y, t, xx, xt, yt, $\cdots$, respectively. The target NPDE (Equation 1) is transformed into a bilinear form using Hirota derivatives or Bell polynomials (Definition 1). This transformation preserves the algebraic structure of soliton equations in a multiplicative sense in Hirota bilinear equation. Using Definition 1, some useful notation are derived as follows:

$$D_tG\cdot F = G_tF - GF_t,$$
$$D_xG\cdot F = G_xF - GF_x,$$
$$D_x^3G\cdot F = G_{xxx}F - 3G_{xx}F_x + 3G_xF_{xx} - GF_{xxx},$$
$$D_x^2F\cdot F = 2(F_{xx}F - F_x^2).$$

Step 2 (Network construction) : Substitute activation function f from Equation 9 to derive algebraic equations in terms of variables such as x, t, y, xy, xt, yt, $F(x,y,z,t),\cdots$ and others. A neural network is designed where certain layers encode bilinear operators by setting the layers in the main models. This step also constructs the trial functions and the loss function built from the basic partial differential equation residual, conservation laws, and boundary/initial conditions (Table 1). Physics-informed constraints are directly embedded into the optimization problem.

Step 3 (Classification via activation functions) : Solve the resulting system of equations to determine the values of the coefficients of the test functions. A hidden layer is introduced to classify the solution type (e.g., lump, breather, rogue wave, or soliton interaction) while also quantifying uncertainty in predictions. The system of algebraic equations are collected and solved to attain the satisfied original equations.

Step 4 (Optimization) : Substitute the test functions back into Equation 9 to construct the exact analytical solutions. Parameters are trained using attained coefficients, minimizing the residual error over collocation points in the domain. This step comprises of solving the algebraic system of equations.

Step 5 (Output solutions) : Verify that the solutions obtained satisfied Equation 1 through direct substitution and validation. The trained BNNM produces exact solutions for high-dimensional NPDEs. This includes multi-soliton interactions, lump–rogue wave collisions, and non-traveling wave patterns. This stage includes checking the satisfaction of the solutions.

Compared with traditional methods, the BNNM can handle higher-dimensional systems, approximate analytically intractable solutions, and adapt to cases with open solutions. This will make a powerful tool for bridging the gap between symbolic integrability and modern machine learning approaches.

3. Hirota bilinear operator of breaking soliton system

The BNNM builds upon Hirota's bilinear operator by embedding the bilinearized form of NPDEs into a neural network framework. The process begins with the bilinearization of the governing NPDE, typically achieved through Hirota's operators or equivalent transformations. Once the equation is bilinearized, the next step involves constructing a specialized neural architecture designed to capture bilinear operations within its layers. Unlike generic neural networks, which often require external constraints to enforce physical consistency, the BNNM integrates the algebraic structure of the equation directly into the system. By assigning probabilities to predefined classes such as lump waves, breather waves, or rogue–soliton interactions, the network can simultaneously solve the NPDE and categorize the nature of its solutions. A compelling demonstration of this approach is provided by the application the (3+1)-dimensional sixth-order BSS equation with variable coefficients. Traditional analytical techniques struggle with such systems due to their complexity and multi-dimensional coupling. In contrast, the BNNM begins with trial functions inspired by known soliton profiles and adaptively tunes with parameters to satisfy the BSS equation throughout the computational domain. Simultaneously, the classification mechanism identifies the resulting solution structure, and manifests as a lump, a breather, or a mixed soliton–rogue wave form. This section will demonstrate the processing steps for original equation shown as the following:

From Equation 1, setting traveling shifting $\xi = kx + sy + ht$, we have

$$hku'' - 6sk^2u'u'' - sk^3u'''' + hpk^3\left(u'\right)^2u'' + qk^5\left(u''u''' + u'.u''''\right) + k^6ru''''' = 0 \quad (5)$$

Let $u = 2w_\xi, w = \ln f$, Equation 5 is transformed to a new form as follows:

$$2hkw_{\xi\xi\xi} - 24sk^2w_{\xi\xi}w_{\xi\xi\xi} - 2sk^3w_{\xi\xi\xi\xi\xi} + 8hpk^3\left(w_{\xi\xi}\right)^2w_{\xi\xi\xi} + 4qk^5\left(w_{\xi\xi\xi}w_{\xi\xi\xi\xi} + w_{\xi\xi}w_{\xi\xi\xi\xi\xi}\right) + 2rk^6w_{\xi\xi\xi\xi\xi\xi\xi} = 0 \quad (6)$$

Integrating on both sides and letting the constant to zero, Equation 6 is rewritten as follows:

$$2hkw_{\xi\xi} - 12sk^2w_{\xi\xi}^2 - 2sk^3w_{\xi\xi\xi\xi} + \frac{8hpk^3}{3}\left(w_{\xi\xi}\right)^3 + 4qk^5w_{\xi\xi}w_{\xi\xi\xi\xi} + 2rk^6w_{\xi\xi\xi\xi\xi\xi} = 0 \quad (7)$$

By simplifying on both sides, Equation 7 is shown as follows:

$$hw_{\xi\xi} - sw_{\xi\xi\xi\xi} - 6sw_{\xi\xi}^2 + 60rw_{\xi\xi}^3 + 30ru_{\xi\xi}u_{\xi\xi\xi\xi} + ru_{\xi\xi\xi\xi\xi\xi} = 0 \quad (8)$$

Using Definition 1, Equation 8 is transformed into Hirota bilinear form as follows:

$$[D_\xi^2 - mD_\xi^4 + nD_\xi^6]f \cdot f = 0 \quad (9)$$

where

$D_x^4 f \cdot f = 2(ff_{xxxx} - 4f_xf_{xxx} + 3f_{xx}^2)$,

$D_x^6 f \cdot f =$

$2(ff_{xxxxxx} - 6f_xf_{xxxxx} + 15f_{xx}f_{xxxx} - 10f_{xxx}^2)$,

$D_x^2 f \cdot f = 2(ff_{xx} - (f_x)^2)$,

and

$$\frac{q}{r} = 15, \frac{p}{r} = \frac{45}{h}, k = 1, m = \frac{s}{h}, n = \frac{r}{h}.$$

4. Solution Construction of breaking soliton system using bilinear neural network method

Many nonlinear physical systems generate solutions with distinct qualitative behaviors such as bright solitons, dark solitons, breathers, rogue waves, or kink waves depending on parameter regimes. While BNNM focuses on learning accurate solution profiles, widely used in machine learning classification tasks, provides an additional mechanism to categorize these solutions. When embedded as the final layer of the BNNM, the hidden layer not only generates the solution profile but also assigns probabilities to different solution types, thereby offering a structured and probabilistic classification of the solution's morphology. BNNM's framework can be trained to approximate the solution surface $u(x, y, t)$ under specified initial and boundary conditions, while simultaneously predicting whether the solution represents a multi-soliton interaction, rogue wave event, or lump wave pattern. This section will illustrate the construction of solution shown as the following:

Case 1: This case designed three layers of neural network model consisting of three neurons of the input layer, one neuron of the hidden layer, and one neuron of the single output layer. Let $f_{11} = a_0 + a_1e^{\xi_1}, \xi_1 := b_1\xi + b_2, \xi = hy + kx + st$

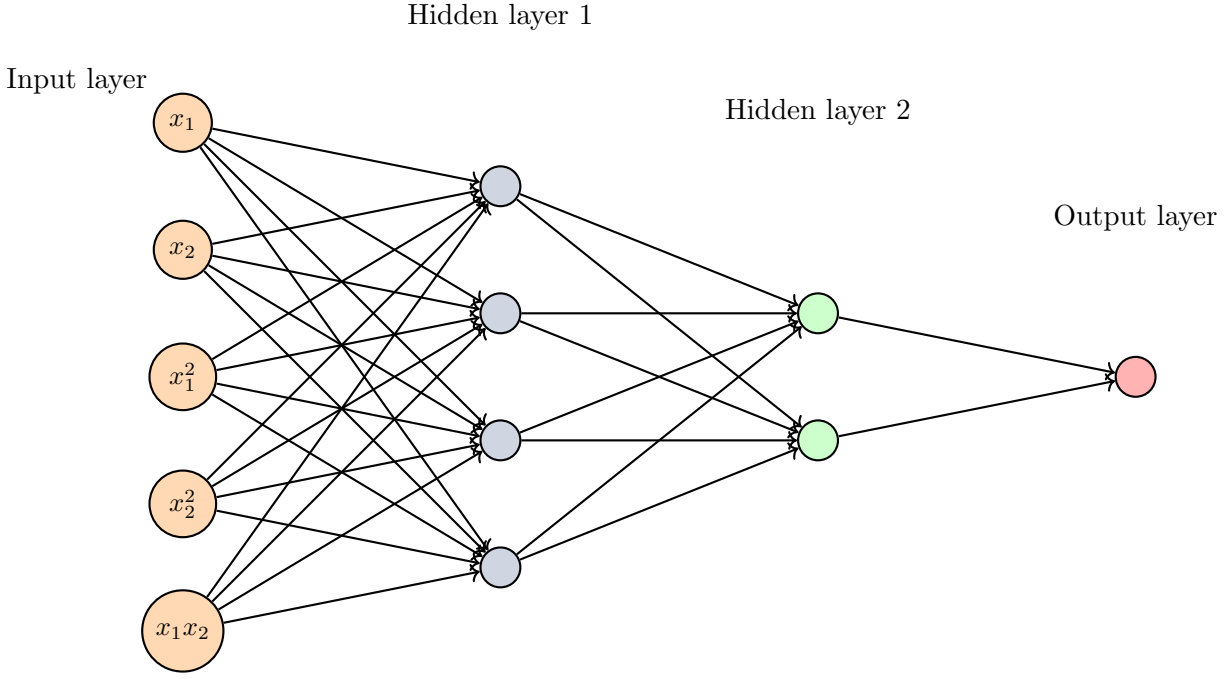

Figure 1. Bilinear neural network architecture used for classification with two hidden layers.

using Case IV in Table 1. Substituting the variables in Equation 9, we gathered the coefficients of trial functions and plugging all into Equation 4 to check the satisfaction, we attain the solution as follows:

$$u_{11} = \frac{2a_1b_1\,\mathrm{e}^{b_1(hy+st+x)+b_2}}{a_0 + a_1\,\mathrm{e}^{b_1(hy+st+x)+b_2}} \tag{10}$$

where $h = \frac{b_1^4 r}{b_1^2-1}, n = \frac{b_1^2 m-1}{b_1^4}, s = \frac{b_1^4 r+h}{b_1^2}$. The graphs of u_{11} are depicted in Figures 2 and 3.

Case 2: This case designed three layers of neural network model consisting of three neurons of the input layers, two of the hidden layers, and one of the output layer. Similarly to Case 1, let $f_{21} = a_0 + a_1 e^{\xi_1+\xi_2}, \xi_1 = b_1\xi + b_2, \xi = hy + kx + st$ using Case IV in Table 1, we obtain the solution as follows:

$$u_{21} = \frac{2a_1\,(b_1+c_1)\,\mathrm{e}^{b_1(hy+st+x)+b_2+\xi_2}}{a_0 + a_1\,\mathrm{e}^{b_1(hy+st+x)+b_2+\xi_2}} \tag{11}$$

where $m = \frac{b_1^4 n+4b_1^3c_1n+6b_1^2c_1^2n+4b_1c_1^3n+c_1^4n+1}{b_1^2+2b_1c_1+c_1^2}, s = \frac{(b_1^4r+4b_1^3c_1r+6b_1^2c_1^2r+4b_1c_1^3r+c_1^4r+h}{b_1^2+2b_1c_1+c_1^2}$,
$h = \frac{r(b_1+c_1)^4}{(b_1+c_1+1)(b_1+c_1-1)}$. The graphs of u_{21} were simulated in the kink solution, similar to Case 1.

Case 3: This case designed three layers of neural network model consisting of three neurons of the input layer, one of the hidden layer, and one of the output layer. Similarly to Case 1, let $f_{31} = a_0 + a_1\cosh(\xi_1), \xi_1 = b_1\xi + b_2, \xi = hy + kx + st$ using Case II in Table 1, we collect the solution as follows:

$$u_{31} = \frac{a_1\sqrt{5}\,\sinh\left(\frac{\sqrt{5}\,(hy+st+x)}{2} + b_2\right)}{a_0 + a_1\cosh\left(\frac{\sqrt{5}\,(hy+st+x)}{2} + b_2\right)} \tag{12}$$

where $m = \frac{5}{4b_1^2}, n = \frac{1}{4b_1^4}, r = \frac{h}{4b_1^4}, s = \frac{5h}{4b_1^2}, b_1 = \pm\frac{\sqrt{5}}{2}$. The graphs of u_{31} are shown in the kink solution, same as Case 1.

Case 4: This case will design three layers of neural network model consisting of three neurons of the input layer, one of the hidden layer, and one of the output layer. Similarly to Case 1, let $f_{41} = a_0 + a_1\cos(\xi_1), \xi_1 = b_1\xi + b_2, \xi = hy + kx + st$ using Case III in Table 1, the solution is shown as follows:

$$u_{41} = \frac{-ia_1\sqrt{5}\,\sin\left(\frac{i\sqrt{5}\,(hy+st+x)}{2} + b_2\right)}{a_0 + a_1\cos\left(\frac{i\sqrt{5}\,(hy+st+x)}{2} + b_2\right)} \tag{13}$$

where $m = \frac{-5}{4b_1^2}, n = \frac{1}{4b_1^4}, r = \frac{h}{4b_1^4}, s = -\frac{5h}{4b_1^2}, b_1 = \pm\frac{\sqrt{5}}{2}$. The graphs of u_{41} are shown in Figures 4 and 5.

Case 5: This case designed three layers of neural network model consisting of three neurons of the input layer, two of the hidden layer, and one of the output layer. Similarly to Case 1, let $f_{51} = a_0 + a_1(e^{\xi_1} + e^{\xi_2})e^{-\xi_2} + a_2e^{2\xi_2}, \xi_1 = b_1\xi + b_2, \xi_2 = c_1\xi + c_2, \xi = hy + kx + st$ using Case VII in Table 1, the solution u_{51} is shown in Table 2, where $b_1 = 5c_1, m = \frac{5}{16c_1^2}, n = \frac{1}{64c_1^4}, r = \frac{h}{64c_1^4}, s = \frac{5h}{16c_1^2}, b_1 = 5c_1, c_1 = \pm\frac{\sqrt{5}}{4}$. Some more

Table 1. Graphical trial functions using for bilinear neural network method

Cases	Names	Trial functions
I	$\tanh - \coth$ [51]	$f_{11} = a_{01} + a_{11}\tanh(k\xi)$ $f_{12} = a_{01} + a_{11}\coth(k\xi)$
II	$\sinh - \cosh$ [51]	$f_{11} = a_{01} + a_{11}\sinh(k\xi)$ $f_{12} = a_{01} + a_{11}\cosh(k\xi)$
III	$\sin - \cos$ [51]	$f_{11} = a_{01} + a_{11}\sin^{\beta}(\mu\xi)$ $f_{12} = a_{01} + a_{11}\cos^{\beta}(\mu\xi)$
IV	1-soliton[51]	$f_{11} = a_{01} + a_{11}e^{k\xi}$
V	3-soliton[51]	$f_{11} = a_{01} + a_{11}e^{k\xi_1} + a_{12}e^{h\xi_2} + a_{13}e^{p\xi_3} + a_{14}e^{q(\xi_1+\xi_2)}$ $+a_{15}e^{r(\xi_2+\xi_3)} + a_{16}e^{l(\xi_1+\xi_3)} + a_{17}e^{m(\xi_1+\xi_2+\xi_3)}$
VI	n-soliton[51]	$f_{11} = a_{01} + \sum_{i=1}^{N} a_i \exp(k_i\xi_i)$ $f_{12} = a_{01} + \sum_{i,j=1}^{N} a_{ij}\exp(k_i(\xi_i + \xi_j))$
VII	Homoclinic test approach[52]	$f_{11} = a_{01} + a_{11}\left(e^{ip\xi_1} + e^{-ip\xi_1}\right)e^{q\xi_2} + a_{12}e^{2q\xi_2}$
VIII	Extended homoclinic test approach[53]	$f_{11} = a_{11}e^{\xi_1} + a_{12}\cos\xi_2 + a_{13}e^{-\xi_1}$ $f_{12} = a_{11}e^{\xi_1} + a_{12}\sin\xi_2 + a_{13}e^{-\xi_1}$
IX	Physics-informed neural network method[54]	$f_{11} = a_{11}e^{\xi_1}(\cos\xi_2 + a_{13}\cosh\xi_1)$ $f_{12} = a_{11}\xi_1^2 + a_{12}\xi_2^2 + a_{13}\cosh\xi_3$
X	Lumps and three-wave[55]	$f_{11} = a_{01} + a_{11}\xi_1^2 + a_{12}\xi_2^2$ $+a_{13}e^{\xi_1} + a_{13}\cos\xi_2 + a_{13}e^{-\xi_1} + a_{16}\cosh\xi_3$ $f_{12} = a_{01} + a_{11}\xi_1^2 + a_{12}\xi_2^2 + a_{13}\cosh\xi_3$
XI	Periodic-soliton, periodic wave[56]	$f_{11} = a_{11}e^{-\xi_1} + a_{12}\tan\xi_2 + a_{13}\tanh\xi_3 + a_{14}e^{\xi_1}$ $f_{12} = a_{11}e^{-\xi_1} + a_{12}\cos\xi_2 + a_{13}\sin\xi_3 + a_{14}e^{\xi_1}$ $f_{13} = a_{11}e^{-\xi_1} + a_{12}\cos\xi_2 + a_{13}\sin\xi_3 + a_{14}\tanh\xi_4 + a_{15}e^{\xi_1}$ $f_{14} = a_{11}e^{-\xi_1} + a_{12}\cos\xi_2 + a_{13}\sin\xi_3 + a_{14}\cosh\xi_4 + a_{15}e^{\xi_1}$
XII	Periodic wave[57]	$f_{11} = a_{11}e^{-\xi_1} + a_{12}\cos\xi_2 + a_{13}\tan\xi_3 + a_{14}\tanh\xi_4$
XIII	Lump-soliton[58]	$f_{11} = a_0 + \xi_1^2 + \xi_2^2 + a_{11}e^{\xi_3}$ $f_{12} = a_0 + \xi_1^2 + \xi_2^2 + a_{11}e^{\xi_3} + a_{12}e^{\xi_4}$ $f_{13} = a_0 + \xi_1^2 + \xi_2^2 + a_{11}\cosh e^{\xi_3}$ $f_{14} = a_0 + \xi_1^2 + \xi_2^2 + a_{11}\cosh e^{\xi_3} + a_{11}\cos e^{\xi_3}$
XIV	k-lump and k-kink[59]	$f_{11} = \xi_1^4 + \xi_1^2 + \xi_2^2 + a_{11}e^{\xi_1}$ $f_{12} = \xi_1^4 + \xi_1^2 + \xi_2^2 + a_{11}e^{\xi_1} + a_{12}e^{\xi_2}$ $f_{13} = \xi_1^4 + \xi_1^2 + \xi_2^2 + a_{11}\cosh\xi_2$ $f_{14} = \xi_1^4 + \xi_1^2 + \xi_2^2 + a_{11}\cos\xi_1 + a_{12}\cos\xi_2$ $f_{15} = a_0 + a_{11}e^{\xi_1}\cos(\xi_1) + a_{12}e^{2\xi_1}$
XV	Rogue, dark, bright soliton[60]	$f_{11} = a_{11}\tanh\xi_1 + a_{12}e^{\xi_2} + a_{13}\xi_3 + a_0,$ $f_{12} = a_{11}e^{\xi_3} + a_{12}e^{-\xi_3} + a_{13}\sin\xi_1 + a_{14}\cos\xi_2 + a_{15}\tanh\xi_4$
XVI	Interference, bright–dark[61]	$f_{11} = a_0 + a_{11}e^{b_0\sin\xi_1 + b_1\cos\xi_2} + a_{12}(a_{13}\sin\xi_1 + a_{14}\cos\xi_2)^2$ $f_{12} = a_0 + a_{11}e^{b_0\sin\xi_1 + b_1\cos\xi_2} + a_{12}(a_{13}\sin\xi_1 + a_{14}\cos\xi_2)^2$ $+a_{15}(a_{16}\sin\xi_1 + a_{17}\cos\xi_2)^2$ $f_{13} = a_0 + a_{11}e^{b_0\xi_3 + b_1e^{\xi_2} + b_2\cos\xi_1} + a_{12}(e^{c_0\xi_3 + c_1e^{\xi_2} + c_2\cos\xi_1})^2$
XVII	Lump-type (by authors)	$f_{11} = a_1e^{\xi_1} + a_2sin(\xi_2) + a_3\cos(-\xi_2) + a_4e^{-\xi_1},$ $f_{12} = a_1e^{\xi_1} + a_2\cos(\xi_2) + a_3sin(-\xi_2) + a_4e^{-\xi_1}$

cases have been found such as $\{b_1 = c_1, m = \frac{16c_1^4n+1}{4c_1^2}, n = n\}, \{b_1 = -c_1, m = \frac{5}{(16c_1^2}, n = \frac{1}{64c_1^4}\}, \{b_1 = 3c_1, m = \frac{16c_1^4n+1}{4c_1^2}, n = n\}, \{b_1 = 5c_1, m = \frac{5}{16c_1^2}, n = \frac{1}{64c_1^4}\}, \{b_1 = 2c_1, m = \frac{5}{4c_1^2}, n = \frac{1}{4c_1^4}\}$.

The graphs of u_{51} are delineated in Figures 6 and 7.

Depending on the cases, the other solutions are found in Table 2, where $b_1 = 2c_1, m = \frac{5}{4c_1^2}, n = \frac{1}{4c_1^4}, c_1 = \pm\frac{\sqrt{5}}{2}$. The solution u_{52} is shown in Table 2, where $s = \frac{(16c_1^4n+1)h}{4c_1^2}, b_1 = 3c_1, h = \frac{16c_1^4r}{4c_1^2-1}$. Solution u_{53}, u_{54} is shown in Table 2, where $b_1 = -c_1, m = \frac{5}{16c_1^2}, n = \frac{1}{64c_1^4}, c_1 = \pm\frac{\sqrt{5}}{4}$. The next solution is attained as follows:

$$u_{55} = \frac{4a_2c_1\,\mathrm{e}^{\frac{(16hy+16x)c_1^2+16c_2c_1+5ht}{8c_1}}}{a_1\,\mathrm{e}^{b_2-c_2} + a_1 + a_2\,\mathrm{e}^{\frac{(16hy+16x)c_1^2+16c_2c_1+5ht}{8c_1}}} + a_0$$

Table 2. Solutions collected from the bilinear neural network method

$u_{51} = \frac{4c_1\left(2a_1\,\mathrm{e}^{(4hy+4st+4x)c_1+b_2-c_2}+a_2\,\mathrm{e}^{(2hy+2st+2x)c_1+2c_2}\right)}{a_1\,\mathrm{e}^{(4hy+4st+4x)c_1+b_2-c_2}+a_1+a_2\,\mathrm{e}^{(2hy+2st+2x)c_1+2c_2}+a_0}$
$u_{52} = \frac{2c_1\left(2a_2\,\mathrm{e}^{\frac{(4hy+4x)c_1^2+4c_2c_1+5ht}{2c_1}}+a_1\,\mathrm{e}^{\frac{(4hy+4x)c_1^2+(4b_2-4c_2)c_1+5ht}{4c_1}}\right)}{a_1\,\mathrm{e}^{\frac{(4hy+4x)c_1^2+(4b_2-4c_2)c_1+5ht}{4c_1}}+a_1+a_2\,\mathrm{e}^{\frac{(4hy+4x)c_1^2+4c_2c_1+5ht}{2c_1}}+a_0}$
$u_{53} = \frac{4c_1\left(a_2\,\mathrm{e}^{\frac{32(t+y)r\,c_1^5+8c_1^3x+8c_1^2c_2-2c_1x-2c_2}{4c_1^2-1}}+a_1\,\mathrm{e}^{\frac{32(t+y)r\,c_1^5+8c_1^3x+(4b_2-4c_2)c_1^2-2c_1x-b_2+c_2}{4c_1^2-1}}\right)}{a_1\,\mathrm{e}^{\frac{32(t+y)r\,c_1^5+8c_1^3x+(4b_2-4c_2)c_1^2-2c_1x-b_2+c_2}{4c_1^2-1}}+a_1+a_2\,\mathrm{e}^{\frac{32(t+y)r\,c_1^5+8c_1^3x+8c_1^2c_2-2c_1x-2c_2}{4c_1^2-1}}+a_0}$
$u_{54} = \frac{4c_1\left(a_2\,\mathrm{e}^{\frac{(16hy+16x)c_1^2+16c_2c_1+5ht}{8c_1}}-a_1\,\mathrm{e}^{\frac{(-16hy-16x)c_1^2+(8b_2-8c_2)c_1-5ht}{8c_1}}\right)}{a_1\,\mathrm{e}^{\frac{(-16hy-16x)c_1^2+(8b_2-8c_2)c_1-5ht}{8c_1}}+a_1+a_2\,\mathrm{e}^{\frac{(16hy+16x)c_1^2+16c_2c_1+5ht}{8c_1}}+a_0}$
$u_{61} = \frac{2a_1b_1\,\mathrm{e}^{b_1(hy+st+x)+b_2}+2a_2c_1\cos(c_1(hy+st+x)+c_2)-2a_3b_1\,\mathrm{e}^{(-hy-st-x)b_1-b_2}}{a_1\,\mathrm{e}^{b_1(hy+st+x)+b_2}+a_2\sin(c_1(hy+st+x)+c_2)+a_3\,\mathrm{e}^{(-hy-st-x)b_1-b_2}}$
$u_{71} = \frac{a_1\sqrt{5}\,\mathrm{e}^{\frac{\sqrt{5}\,(hy+st+x)}{2}+b_2}+a_2\sqrt{5}\,\mathrm{e}^{\frac{\sqrt{5}\,(hy+st+x)}{2}+c_2}+2a_3\sqrt{5}\,\mathrm{e}^{\sqrt{5}\,(hy+st+x)+b_2+c_2}}{a_0+a_1\,\mathrm{e}^{\frac{\sqrt{5}\,(hy+st+x)}{2}+b_2}+a_2\,\mathrm{e}^{\frac{\sqrt{5}\,(hy+st+x)}{2}+c_2}+a_3\,\mathrm{e}^{\sqrt{5}\,(hy+st+x)+b_2+c_2}}$
$u_{81} = -\frac{2c_1(i\cosh(-i\xi c_1+b_2)a_3+ia_3\sinh(-i\xi c_1+b_2)+i\cos\xi_2+\sin\xi_2)}{\cos\xi_2+\cosh(-i\xi c_1+b_2)a_3}$
$u_{91} = \frac{2a_1b_1\,\mathrm{e}^{b_1\xi+b_2}+2b_2c_1\cos(c_1\xi+c_2)-2a_3c_1\sin(c_1\xi+c_2)-2a_4b_1\,\mathrm{e}^{-\xi b_1-b_2}}{a_1\,\mathrm{e}^{b_1\xi+b_2}+b_2\sin(c_1\xi+c_2)+a_3\cos(c_1\xi+c_2)+a_4\,\mathrm{e}^{-\xi b_1-b_2}}$

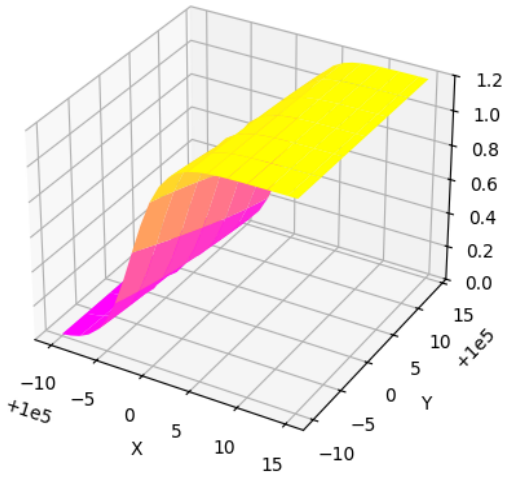

Figure 2. Kink solution u_{11} when $b_{11} = 0.6, b_{12} = 0.3, a_0 = 0.2, a_1 = 0.3, r = 0.5, t = 0.5$.

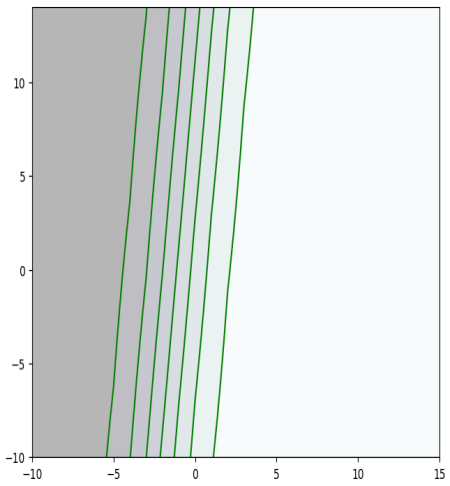

Figure 3. Contour graph of solution u_{11} when $b_{11} = 0.6, b_{12} = 0.3, a_0 = 0.2, a_1 = 0.3, r = 0.5, t = 0.5$.

where $b_1 = c_1, m = \frac{16nc_1^4+1}{4c_1^2}, c_1 = \pm\frac{\sqrt{5}}{4}$. The graphs of u_{52} are shown in Figures 8 and 9.

Case 6: This case designed three layers of neural network model consisting of three neurons of the input layer, two of the hidden layer, and one of the output layer. Similarly to Case 1, let $f_{61} = a_1e^{\xi_1}+a_2sin(\xi_2)+a_3e^{-\xi_1}, \xi_1 = b_1\xi+b_2, \xi_2 = c_1\xi+c_2, \xi = hy+kx+st$ using Case VIII in Table 1, the solution u_{61} is shown in Table 2, where $m = -\frac{16c_1^4n+1}{4c_1^2}, s = -\frac{(16c_1^4n+1)h}{4c_1^2}, h = -\frac{16c_1^4r}{4c_1^2+1}, b_1 = c_1i$. The graphs of u_{61} are shown in Figures 10 and 11.

Case 7: This case designed three layers of neural network model consisting of three neurons of the input layers, two of the hidden layers, and one of the output layer. Similarly to Case 1, let $f_{71} = a_0 + a_1e^{\xi_1} + a_2e^{\xi_2} + a_3e^{\xi_1+\xi_2}, \xi_1 = b_1\xi+b_2, \xi_2 = c_1\xi+c_2, \xi = hy+kx+st$ using Case VI in Table 1, the solution u_{71} is shown in Table 2, where $m = \frac{5}{4c_1^2}, n = \frac{1}{4c_1^4}, r = \frac{h}{4c_1^4}, s = \frac{5h}{4c_1^2}, b_1 = \pm c_1, c_1 = \frac{\sqrt{5}}{2}$. The graphs of u_{71} are shown in Figures 12 and 13.

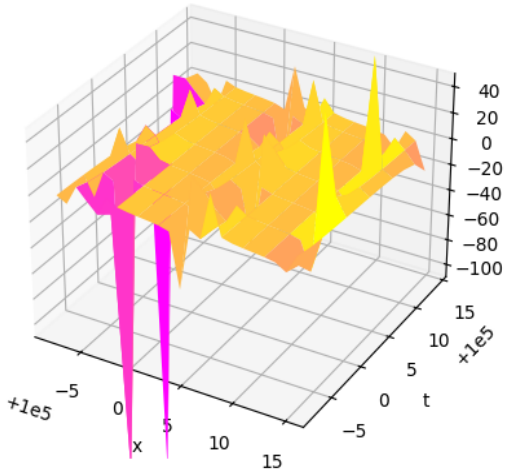

Figure 4. Rogue solution u_{41} when $b_{11} = 0.6, b_{12} = 0.3, a_0 = 0.2, a_1 = 0.3, r = 0.5, t = 0.5$.

Figure 5. Contour graph of solution u_{41} when $b_{11} = 0.6, b_{12} = 0.3, a_0 = 0.2, a_1 = 0.3, r = 0.5, t = 0.5$.

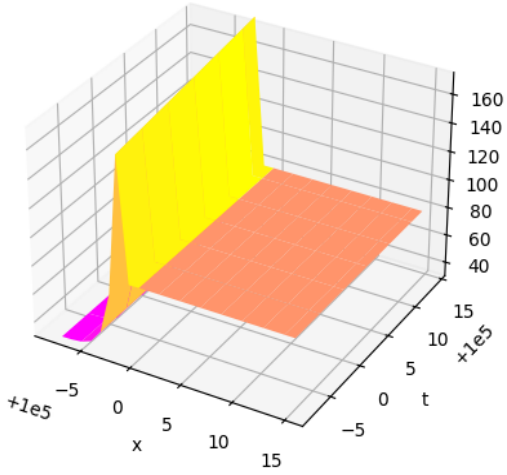

Figure 6. Peak solution u_{51} when $b_{11} = 0.6, b_{12} = 0.3, a_0 = 0.2, a_1 = 0.3, r = 0.5, t = 0.5, h = 1.5$.

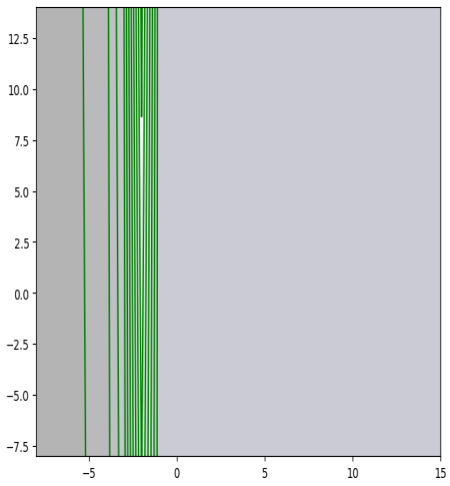

Figure 7. Contour graph of solution u_{51} when $b_{11} = 0.6, b_{12} = 0.3, a_0 = 0.2, a_1 = 0.3, r = 0.5, t = 0.5$.

Case 8: This case designed three layers of neural network model consisting of three neurons of the input layers, two of the hidden layers, and one of the output layer. Similarly to Case 1, let $f_{21} = a_1 e^{\xi_1}(\cos(\xi_2) + a_3 \cosh(\xi_1)), \xi_1 = b_1\xi + b_2, \xi_2 = c_1\xi + c_2, \xi = hy + kx + st$ using Case IX in Table 1, the solution u_{81} is performed in Table 2, where $m = -\frac{16c_1^4 n+1}{4c_1^2}, b_1 = -ic_1, s = -\frac{(16c_1^4 n+1)h}{4c_1^2}, b_1 = c_1 i, h = -\frac{16c_1^4 r}{4c_1^2+1}$. The graphs of u_{81} are shown in Figures 14 and 15.

Case 9: This case designed three layers of neural network model consisting of three neurons of the input layers, two of the hidden layers, and one of the output layer. Similarly to Case 1, let $f_{21} = a_1 e^{\xi_1} + a_2 sin(\xi_2) + a_3 \cos(-\xi_2) + a_4 e^{-\xi_1}, \xi_1 = b_1\xi + b_2, \xi_2 = c_1\xi + c_2, \xi = hy + kx + st$ using Case XVII in Table 1, the solution u_{91} is shown in Table 2, where $m = -\frac{16c_1^4 n+1}{4c_1^2}, b_1 = \pm c_1 i, s = -\frac{(16c_1^4 n+1)h}{4c_1^2}, h = -\frac{16c_1^4 r}{4c_1^2+1}$. The graphs of u_{91} are shown in Figures 16 and 17.

5. Graphical performance of the solutions

To assess the expressive power of the proposed bilinear neural network-based construction, analyzing the simulated fields associated with cases was performed. Across all cases, two complementary views were employed: a three-dimensional surface to emphasize amplitude and local geometry, and a contour map to emphasize level set topology and interaction footprints.

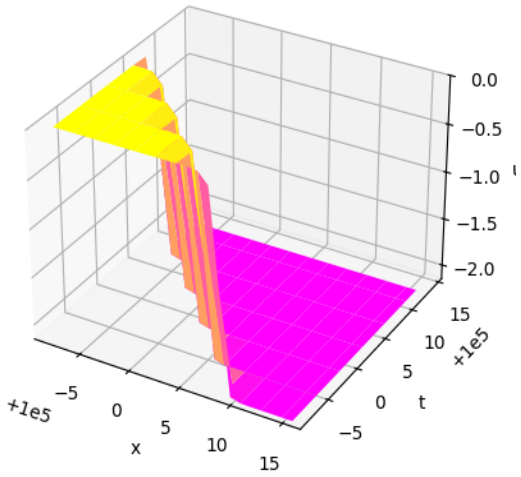

Figure 8. Anti-kink solution u_{52} when $c_{11} = -\frac{\sqrt{5}}{2}, b_{12} = 0.3, a_0 = 0.2, a_1 = 0.4, r = 0.1, t = 0.1, c_{12} = 0.2, h = 0.1, b_{11} = 2c_{11}, a_2 = 0.1$.

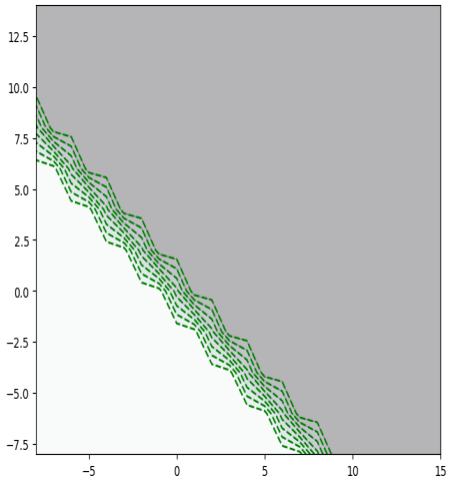

Figure 9. Contour graph of solution u_{52} when $c_{11} = -\frac{\sqrt{5}}{2}, b_{12} = 0.3, a_0 = 0.2, a_1 = 0.4, r = 0.1, t = 0.1, c_{12} = 0.2, h = 0.1, b_{11} = 2c_{11}, a_2 = 0.1$.

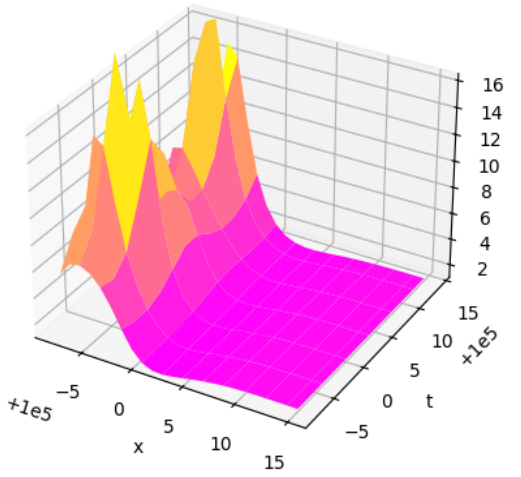

Figure 10. Breather solution u_{61} when $b_{11} = 0.6, b_{12} = 0.3, a_0 = 0.2, a_1 = 0.3, r = 0.5, t = 0.5, h = 1.5, a_2 = 0.2, a_3 = 0.1$.

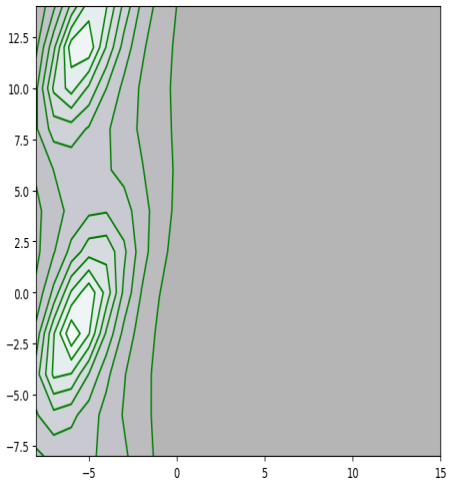

Figure 11. Contour graph of solution u_{61} when $b_{11} = 0.6, b_{12} = 0.3, a_0 = 0.2, a_1 = 0.3, r = 0.5, t = 0.5, a_2 = 0.2, a_3 = 0.1$.

Together, these perspectives diagnosed waveform class (kink, lump, rogue, periodic), anisotropy, and parameter sensitivity with minimal ambiguity[30].

Kink profiles Figures 2 & 3: The one-soliton (kink) produced by the simplest exponential trial exhibited a monotone transition between two asymptotic plateaus, with the maximum gradient aligned along a tilted ridge governed by the traveling coordinate $\xi = hy + kx + st$. The contour plot revealed nearly parallel isolines in the far field, confirming the single-front nature of the solution. Varying a_0 shifted the baseline, a_1 controlled the jump height, and b_1 set the inverse width. These dependencies are visually linear in the surface slope and linearly spaced contours.

Peak and plateau regulation Figures 6 & 7: In this case, the mixture $u(\xi_1, \xi_2) = (e^{\xi_1} + e^{\xi_2})e^{-\xi_2} + e^{2\xi_2}$ sharpened the crest and flattened the shoulders. The three-dimensional surface showed a taller, narrower core with gentle terraces extending along the transverse direction. The contour view compressed near the peak (dense level sets) and dilated along the terraces (sparse level sets), visually encoding anisotropy.

Hybrid morphologies Figures 10, 11, 14, & 15: The Spike-typefigures arose when sinusoidal components blended with exponentials. A localized spike (rogue-like amplification) riding on a kink-like background was observed; in contours, this presented as nested, tightly spaced loops centered atop gradually drifting lines.

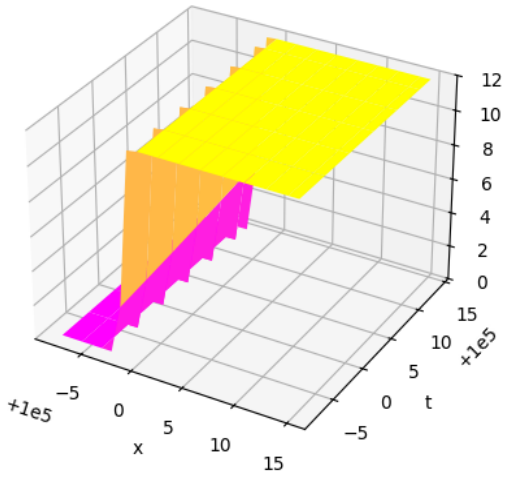

Figure 12. Lump-type solution u_{71} when $b_{11} = 0.6, b_{71} = 0.3, a_0 = 0.2, a_1 = 0.3, r = 0.5, t = 0.5$.

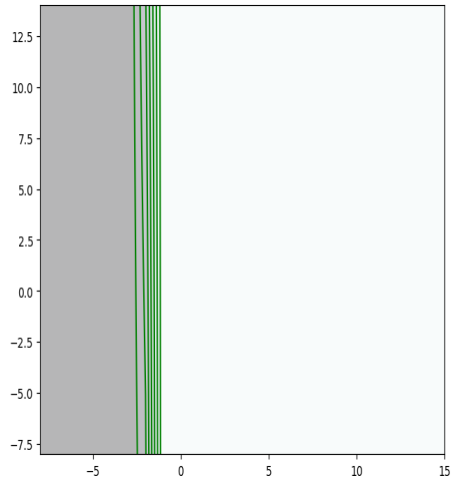

Figure 13. Contour graph of solution u_{71} when $b_{11} = 0.6, b_{12} = 0.3, a_0 = 0.2, a_1 = 0.3, r = 0.5, t = 0.5$.

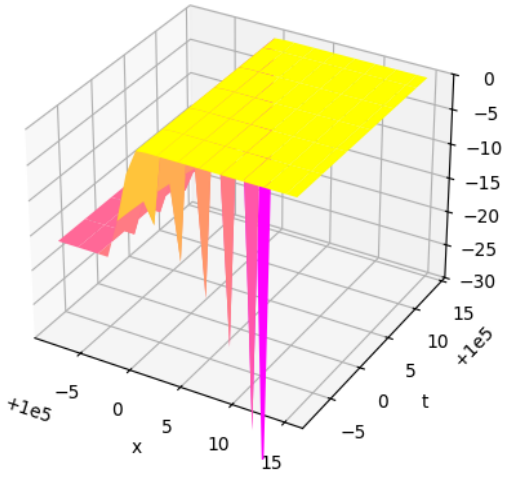

Figure 14. Spike-type solution u_{81} when $b_{11} = 0.6, b_{12} = 0.3, a_0 = 0.2, a_1 = 0.3, r = 0.5, t = 0.5, a_2 = 0.2, a_3 = 0.1$.

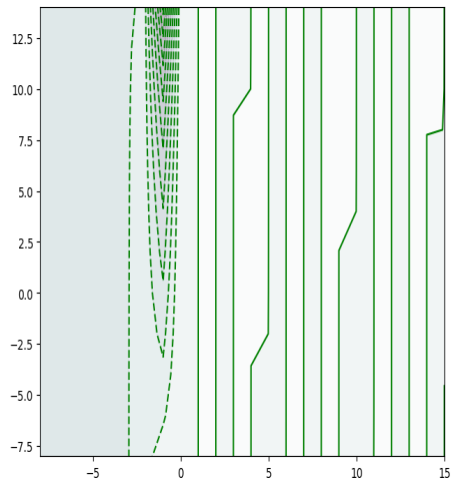

Figure 15. Contour graph of solution u_{81} when $b_{11} = 0.6, b_{12} = 0.3, a_0 = 0.2, a_1 = 0.3, r = 0.5, t = 0.5, a_2 = 0.2, a_3 = 0.1$.

Lump features and mixed interactions Figures 12, 13, 16, & 17: Lump-like structures (Cases 7 and 9) were identifiable by algebraically decaying wings and a quasi-circular footprint in contours, interaction terms introduce ellipticity and tilt. In Figures 14, the addition of a counter-propagating exponential $e^{-\xi_1}$ generated a saddle-like deformation near the lump, visible as a peanut contour.

6. Limitations and discussions

Using the BNNM, exact analytical solutions were primarily expressed in terms of exponential and hyperbolic activation functions, yielding classical soliton and periodic wave structures[62]. The subsequent investigation on the Boussinesq equation emphasized the sensitivity of solution accuracy and stability to network depth and neuron configurations, revealing that architectural optimization significantly influences convergence behavior[63]. Furthermore, some studies have focused on the dynamical stability and chaotic characteristics of soliton solutions in physical and integrable systems. The current approach places greater emphasis on the systematic generation of exact analytical forms and their classification using neural bilinear structures[64,65]. Although the BNNM employed in this study provides a straightforward and systematic procedure for constructing exact solutions of the sixth-order BSS, several limitations should be noted. First, the approach relies on specific transformations and ansatz forms, which may restrict the class of admissible solutions. Consequently, certain types of localized

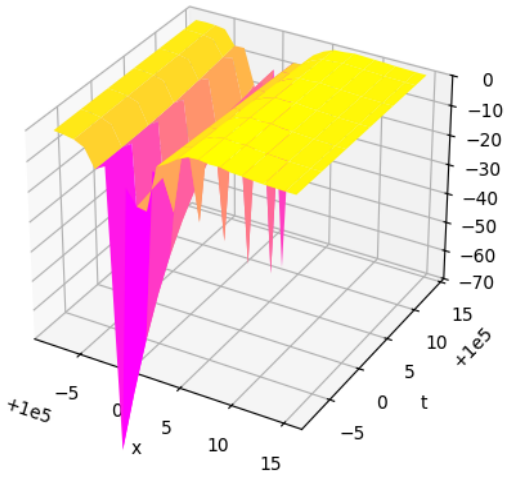

Figure 16. Lump-type solution u_{91} when $b_{11} = 0.6, b_{12} = 0.3, a_0 = 0.2, a_1 = 0.3, r = 0.5, t = 0.5, a_2 = 0.2, a_3 = 0.1, a_4 = 0.5$.

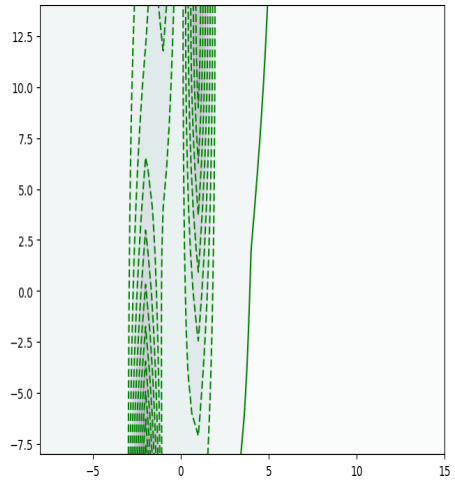

Figure 17. Contour graph of solution u_{91} when $b_{11} = 0.6, b_{12} = 0.3, a_0 = 0.2, a_1 = 0.3, r = 0.5, t = 0.5, a_2 = 0.2, a_3 = 0.1, a_4 = 0.5$.

structures or multi-soliton interactions might not be captured within this framework. Second, the method is primarily analytical and does not directly address the stability or physical realizability of the obtained solutions. By providing a stability analysis, the practical applicability of these solutions to real-world wave phenomena depends on the given activation functions. Third, the parameter constraints required for the existence of exact solutions can limit the range of physical scenarios modeled by the equation. From a broader perspective, the results highlight the richness of the sixth-order BSS, revealing multiple families of waveforms. However, using numerical simulations, and experimental applications on Maple still requires further investigation for variety of test functions. Based on the fundamental functions, the test functions are constructed and substituted to original functions that could prevent the establishment of the general methodology.

7. Conclusion

In this study, the sixth-order BSS was investigated through analytical and computational techniques. By applying the Hirota bilinear form and expansion methods, a range of exact solutions were derived, including multi-soliton, breather, lump, and mixed-type wave structures. The analyzed roadmap demonstrated the rich dynamics of BSS using given test functions under various parameter conditions, cover both the stability and interaction properties of solitons in higher-order nonlinear models. Graphical simulations further validated the obtained solutions, illustrating physical relevance in describing nonlinear wave propagation across three dimensions. The visual performance confirmed that the bilinear expansion method provides not only practical interpretability of the wave structures but also investigates their behavior. Overall, the results emphasize the applicability of bilinear expansion methods and modern extensions, providing new classes of solutions in complex nonlinear systems. These results contribute to the deeper understanding of breaking soliton dynamics and support future applications in mathematical physics, optical communications, fluid dynamics, and other areas.

Acknowledgments

We sincerely appreciate the financial research support of the Posts and Telecommunications Institute of Technology in Ho Chi Minh City, Vietnam, and for providing the necessary resources, a conducive research environment that contributed significantly to the success of this study.

Funding

Posts and Telecommunications Institute of Technology in Ho Chi Minh City, Vietnam Number 999/QĐ-HV.

Conflict of interest

The authors declare no conflict of interest.

Author contributions

Conceptualization: Nguyen Minh Tuan
Investigation: Nguyen Minh Tuan, Nguyen Hong Son
Methodology: All authors
Formal analysis: Nguyen Minh Tuan
Writing – original draft: Nguyen Minh Tuan,

Nguyen Hong Son
Writing – review & editing: Huynh Trong Thua

Availability of data

Not applicable.

AI tools statement

All authors confirm that no AI tools were used in the preparation of this manuscript.

References

1. Almusawa H, Jhangeer A, Hussain Z. Observation on different dynamics of breaking soliton equation by bifurcation analysis and multistability theory. *Results in Phy.* 2022;36:105364. https://doi.org/10.1016/j.rinp.2022.105364
2. Chen X, Xia T, Zhu L. A (2 + 1)-Dimensional integrable breaking soliton equation and its Algebro-Geometric solutions. *Mathematics.* 2024;12(13):2034. https://doi.org/10.3390/math12132034
3. Kumar S, Almusawa H, Dhiman SK. A study of Bogoyavlenskii's (2+1)-dimensional breaking soliton equation: Lie symmetry, dynamical behaviors and closed-form solutions. *Results in Phy.* 2021;29:104793. https://doi.org/10.1016/j.rinp.2021.104793
4. Kumar S, Niwas M, Osman MS, Abdou MA. Abundant different types of exact soliton solution to the (4+1)-dimensional Fokas and (2+1)-dimensional breaking soliton equations. *Commun Theor Phys.* 2021;73(10):105007. https://doi.org/10.1088/1572-9494/ac11ee
5. Shang Y. Abundant explicit non-traveling wave solutions for the (2+1)-dimensional breaking soliton equation. *Appl Math Lett.* 2022;131:108029. https://doi.org/10.1016/j.aml.2022.108029
6. Li C, Zhao M. Analytical solutions of the (2 + 1) -dimensional space–time fractional Bogoyavlenskii's breaking soliton equation. *Appl Math Lett.* 2018;84:13–18. https://doi.org/10.1016/j.aml.2018.04.011
7. Tariq KU-H, Seadawy AR. Bistable Bright-Dark solitary wave solutions of the (3 + 1)-dimensional Breaking soliton, Boussinesq equation with dual dispersion and modified Korteweg–de Vries–Kadomtsev–Petviashvili equations and their applications. *Results in Phy.* 2017;7:1143–1149. https://doi.org/10.1016/j.rinp.2017.03.001
8. Yan X-W, Tian S-F, Dong M-J, Zhou L, Zhang T-T. Characteristics of solitary wave, homoclinic breather wave and rogue wave solutions in a (2+1)-dimensional generalized breaking soliton equation. *Comput Math Appl.* 2018;76(1):179–186. https://doi.org/10.1016/j.camwa.2018.04.013
9. Hasan FL, Abdoon MA, Saadeh R, Qazza A, Almutairi DK. Exploring analytical results for (2+1) dimensional breaking soliton equation and stochastic fractional Broer-Kaup system. *AIMS Math.* 2024;9(5):11622–11643. https://doi.org/10.3934/math.2024570
10. Chen H, Zhu Q, Qi J. Further results about the exact solutions of conformable space–time fractional Boussinesq equation (FBE) and breaking soliton (Calogero) equation. *Results in Phy.* 2022;37:105428. https://doi.org/10.1016/j.rinp.2022.105428
11. Wazwaz AM. Generalized (2+1)-dimensional breaking soliton equation. *TWMS J. App. Eng. Math.* 2011;1(1),69-74.
12. Xu G. Integrability of a (2+1)-dimensional generalized breaking soliton equation. *Applied Mathematics Letters.* 2015;50:16–22. https://doi.org/10.1016/j.aml.2015.05.015
13. Hu X, Lin S, Wang L. Integrability, multiple-cosh, lumps and lump-soliton solutions to a (2+1)-dimensional generalized breaking soliton equation. *Commun Nonlinear Sci Numer Simul.* 2020;91:105447. https://doi.org/10.1016/j.cnsns.2020.105447
14. Dong M-J, Tian S-F, Wang X-B, Zhang T-T. Lump-type solutions and interaction solutions in the (3 + 1)-dimensional potential Yu–Toda–Sasa–Fukuyama equation. *Anal Math Phys.* 2019;9(3):1511–1523. https://doi.org/10.1007/s13324-018-0258-0
15. Alzahrani S, Alzahrani T. Multiple solitons with bifurcations, lump waves, M-shaped and interaction solitons of three component generalized (3+1)-dimensional Breaking soliton system. *AIMS Math.* 2023;8(8):17803–17826. https://doi.org/10.3934/math.2023908
16. Hosseini K, Seadawy AR, Mirzazadeh M, Eslami M, Radmehr S, Baleanu D. Multiwave, multicomplexiton, and positive multicomplexiton solutions to a (3 + 1)-dimensional generalized breaking soliton equation. *Alex Eng J.* 2020;59(5):3473–3479. https://doi.org/10.1016/j.aej.2020.05.027
17. Cheng W, Li B, Chen Y. Nonlocal symmetry and exact solutions of the (2+1)- dimensional breaking soliton equation. *Commun Nonlinear Sci Numer Simul.* 2015;29(1–3):198–207. https://doi.org/10.1016/j.cnsns.2015.05.007
18. Plaatjie K, Khalique CM. On the solutions and conservation laws of the 2D breaking soliton equation of fluid mechanics. *Partial Differ Equ Appl Math.* 2021;4:100198. https://doi.org/10.1016/j.padiff.2021.100198
19. Osman MS. On multi-soliton solutions for the (2 + 1) -dimensional breaking soliton equation with variable coefficients in a graded-index waveguide. *Comput Math Appl.* 2018;75(1):1–6. https://doi.org/10.1016/j.camwa.2017.08.033

20. Yao Y, Chen D, Zeng Y. Soliton solutions for a -dimensional breaking soliton equation with self-consistent sources. *Nonlinear Anal Theory Methods Appl.* 2010;72(1):57–64. https://doi.org/10.1016/j.na.2009.06.066
21. Cerdik Yaslan H, Girgin A. SITEM for the conformable space-time fractional Boussinesq and (2 + 1)-dimensional breaking soliton equations. *J Ocean Eng Sci.* 2021;6(3):228–236. https://doi.org/10.1016/j.joes.2020.11.010
22. Zhu X, Zuo D. Some (2 + 1) -dimensional nonlocal 'breaking soliton'-type systems. *Appl Math Lett.* 2019;91:181–187. https://doi.org/10.1016/j.aml.2018.12.011
23. Niwas M, Kumar S, Kharbanda H. Symmetry analysis, closed-form invariant solutions and dynamical wave structures of the generalized (3+1)-dimensional breaking soliton equation using optimal system of Lie subalgebra. *J Ocean Eng Sci.* 2022;7(2):188–201. https://doi.org/10.1016/j.joes.2021.08.002
24. Tao Z-L. Solving the breaking soliton equation by He's variational method. *Comput Math Appl.* 2009;58(11–12):2395–2397. https://doi.org/10.1016/j.camwa.2009.03.033
25. Da-Quan X. Symmetry reduction and new non-traveling wave solutions of (2+1)-dimensional breaking soliton equation. *Commun Nonlinear Sci Numer Simul.* 2010;15(8):2061–2065. https://doi.org/10.1016/j.cnsns.2009.08.013
26. Zhao Z, Dai Z, Mu G. The breather-type and periodic-type soliton solutions for the (2+1)-dimensional breaking soliton equation. *Comput Math Appl.* 2011;61(8):2048–2052. https://doi.org/10.1016/j.camwa.2010.08.065
27. Wang J-M, Yang X. Theta-function Solutions to the (2+l)-Dimensional Breaking Soliton Equation. *Phys Lett.* 2011;28(9):090203. https://doi.org/10.1088/0256-307X/28/9/090203
28. Yıldırım Y, Yaşar E. A (2+1)-dimensional breaking soliton equation: Solutions and conservation laws. *Chaos Sol Frac.* 2018;107:146–155. https://doi.org/10.1016/j.chaos.2017.12.016
29. Ting S, Xian-Guo G, Yun-Ling M. Wronskian Form of N -Soliton solution for the (2+1)-Dimensional breaking soliton equation. *Phy Lett.* 2007;24(2):305–307. https://doi.org/10.1088/0256-307X/24/2/001
30. Tuan NM, Meesad P, Son NH. New Solutions of Breaking Soliton Equation Using Softmax Method. *J Appl Math.* 2025;13. https://doi.org/10.1155/jama/8810599
31. Gai L, Ma W-X, Sudao B. Abundant multilayer network model solutions and bright-dark solitons for a (3 + 1)-dimensional p-gBLMP equation. *Nonlinear Dyn.* 2021;106(1):867–877. https://doi.org/10.1007/s11071-021-06864-8
32. Demiray ST, Baskonus HM, Bulut H. Application of the HPM for nonlinear (3+ 1)-dimensional breaking soliton equation. *Math Eng Sci Aerosp.* 2014;5(1):127-133.
33. Davies Adeyemo O, Masood Khalique C. Computational approach in obtaining analytic solutions of a generalized nonlinear breaking soliton equation with applications in engineering and physics. *J Taibah Univ Sci.* 2024;18(1):2331984. https://doi.org/10.1080/16583655.2024.2331984
34. Gai L, Wu W, Ding T, Qian Y. Lump wave solutions, lump-stripe soliton inelastic collision phenomena and rogue-type wave solutions for a generalized breaking soliton system in (3+1)-dimensions. *Wave Motion.* 2024;124:103243. https://doi.org/10.1016/j.wavemoti.2023.103243
35. Gai L, Ma W-X, Li M. Lump-type solutions, rogue wave type solutions and periodic lump-stripe interaction phenomena to a (3 + 1)-dimensional generalized breaking soliton equation. *Physics Letters A.* 2020;384(8):126178. https://doi.org/10.1016/j.physleta.2019.126178
36. Zhou H. Parallel Physics-Informed Neural Networks Method with Regularization Strategies for the Forward-Inverse Problems of the Variable Coefficient Modified KdV Equation. *J Syst Sci Complex.* 2024;37(2):511–544. https://doi.org/10.1007/s11424-024-3467-7
37. Ma S-H, Fang J-P, Zheng C-L. New exact solutions of the (2+1)-dimensional breaking soliton system via an extended mapping method. *Chaos Sol Frac.* 2009;40(1):210–214. https://doi.org/10.1016/j.chaos.2007.07.043
38. Gao Y-T, Tian B. New family of overturning soliton solutions for a typical breaking soliton equation. *Comput Math Appl.* 1995;30(12):97–100. https://doi.org/10.1016/0898-1221(95)00176-Y
39. Wazwaz A-M. Integrable (2+1)-dimensional and (3+1)-dimensional breaking soliton equations. *Phy Scri.* 2010;81(3):035005. https://doi.org/10.1088/0031-8949/81/03/035005
40. Tuan NM, Phayung M. A novel softmax method for solving second Benney-Luke equation. *J. Comput Appl Math.* 2025;472(2025):116791. https://doi.org/10.1016/j.cam.2025.116791
41. Tuan NM, Meesad P. New solutions of sixth-order Benney-Luke equation using bilinear neural network method. *Z. Angew Math Phys.* 2025;76(4):133. https://doi.org/10.1007/s00033-025-02516-8
42. Tuan NM, Thuy PTT, Cuong HHN, Hien NT. On Determining Multiple Languages through Technological Examination for Conservation Management Using Machine Learning. *Forum Linguist Stud.* 2025;7(5):Article 5. https://doi.org/10.30564/fls.v7i5.9110
43. Tuan NM, Son NH. Hirota Bilinear Performance on Hirota–Satsuma–Ito Equation Using Bilinear Neural Network Method. *Int J Appl Comput Math.* 2025;11(121). https://doi.org/10.1007/s40819-025-01933-7
44. Tuan NM. A Novel Softmax Building Method for Finding Solutions of Benney-Luke Equation. *Int*

J Theor Phys. 2025;64:145.
https://doi.org/10.1007/s10773-025-06002-9

45. Tuan, N. M., & Son, N. H. A New Softmax Method Performance for Solving Chaffee-Infante Equation. *Int J Math Comput Sci.* 2025;20(3):743–749.
https://doi.org/10.69793/ijmcs/03.2025/tuan
46. Tuan NM, Alqurashi MS, Alderremy AA, Mahmoud EE. Repercussions of concentration and thermal transport of magnetized radiative ternary nanofluid over spinning sphere: Three neural layers modeling. *J Radiat Res Appl Sci.* 2025;18(2):101508.
https://doi.org/10.1016/j.jrras.2025.101508
47. Tuan NM, Meesad P. A bilinear neural network method for solving a generalized fractional (2+1)-Dimensional konopelchenko-Dubrovsky-Kaup-Kupershmidt equation. *Int J Theor Phys.* 2025;64(2025):17.
https://doi.org/10.1007/s10773-024-05855-w
48. Tuan NM, Meesad P. Bilinear Recurrent Neural Network for a Modified Benney-Luke Equation. *Int J Appl Comput Math.* 2025;11(2):35.
https://doi.org/10.1007/s40819-025-01851-8
49. Tuan NM, Meesad P, Nguyen HHC. English–Vietnamese Machine Translation Using Deep Learning for Chatbot Applications. *SN Comput Sci.* 2023;5(1):5.
https://doi.org/10.1007/s42979-023-02339-2
50. Tuan NM, Meesad P, Hieu DV, Cuong NHH, Maliyaem M. On students' sentiment Prediction based on deep learning: applied information literacy. *SN Comput Sci.* 2024;5(7):928.
https://doi.org/10.1007/s42979-024-03281-7
51. Wazwaz A-M. Partial differential equations and solitary waves theory. *HigH Edu Press.* Springer. 2009.
52. Dai Z, Liu J, Li D. Applications of HTA and EHTA to YTSF Equation. *Appl Math Comput.* 2009;207(2):360–364.
https://doi.org/10.1016/j.amc.2008.10.042
53. Zhao Z, Dai Z, Han S. The EHTA for nonlinear evolution equations. *Appl Math Comput.* 2010;217(8):4306-4310.
https://doi.org/10.1016/j.amc.2010.09.069
54. Miao Z, Chen Y. Physics-informed neural networks method in high-dimensional integrable systems. *Mod Phys Lett B.* 2022;36(01):2150531.
https://doi.org/10.1142/S021798492150531X
55. Wang X, Bilige S. Novel interaction phenomena of the (3+1)-dimensional Jimbo–Miwa equation. *Commun Theor Phys.* 2020;72(4):045001.
https://doi.org/10.1088/1572-9494/ab690c
56. Shen J-L, Wu X-Y. Periodic-soliton and periodic-type solutions of the (3+1)-dimensional Boiti–Leon–Manna–Pempinelli equation by using BNNM. *Nonlinear Dynamics.* 2021;106(1):831–840.
https://doi.org/10.1007/s11071-021-06848-8
57. Feng Y, Bilige S. Various rational solutions and rogue wave solutions of extended (2+1)-dimensional Calogero-Bogoyavlenskii-Schiff-like equation. Authorea. Preprint posted 2020.
https://doi.org/10.22541/au.160407386.60382756/v1
58. Hong B, Wang J. Exact Solutions for the Generalized Atangana-Baleanu-Riemann Fractional (3 + 1)-Dimensional Kadomtsev–Petviashvili Equation. *Symmetry.* 15(1), 3.
https://doi.org/10.3390/sym15010003
59. Gu Y, Malmir S, Manafian J, Ilhan OA, Alizadeh A, Othman AJ. Variety interaction between k -lump and k -kink solutions for the (3+1)-D Burger system by bilinear analysis. *Res in Phy.* 2022;43:106032.
https://doi.org/10.1016/j.rinp.2022.106032
60. Abdeljabbar A, Roshid H-O, Aldurayhim A. Bright, Dark, and Rogue Wave Soliton Solutions of the Quadratic Nonlinear Klein-Gordon Equation. *Symmetry.* 2022;14(6): 1223.
https://doi.org/10.3390/sym14061223
61. Zhang R-F, Li M-C, Cherraf A, Vadyala SR. The interference wave and the bright and dark soliton for two integro-differential equation by using BNNM. *Nonlinear Dynamics.* 2023;111(9):8637-8646.
https://doi.org/10.1007/s11071-023-08257-5
62. Isah MA, Yokus A, Kaya D. A bilinear neural network method for obtaining exact analytical solutions of nonlinear evolution equations with application to the kdv equation. 2024.
https://doi.org/10.22034/kjm.2024.396918.2865
63. Isah M A, Yokus A, Kaya D. Exploring the influence of layer and neuron configurations on Boussinesq equation solutions via a bilinear neural network framework. *Nonlinear Dyn.* 2024;112(15):13361–13377.
https://doi.org/10.1007/s11071-024-09708-3
64. Ullah MS, Akter R. Soliton dynamics and stability analysis of a double-chain DNA model with various chaos detection tools. *Sci Rep.* 2025;16(1):1164.
https://doi.org/10.1038/s41598-025-30779-8
65. Usman T, Ullah MS. Analytical solutions and chaotic insights into the Hirota-Maccari system. *Sci Rep.* 2025;15(1):43540.
https://doi.org/10.1038/s41598-025-27419-6

Nguyen Minh Tuan *is a computer scientist from Ho Chi Minh City, Vietnam, currently affiliated with the Posts and Telecommunications Institute of Technology (PTIT). He earned his Ph.D. in Applied Mathematics in the direction of Computer Science from King Mongkut's University of Technology North Bangkok (KMUTNB), Thailand. He also holds a Master's degree in Mathematics from the University of Science,*

Ho Chi Minh City, and a Bachelor's degree in Mathematics and Computer Science from Can Tho University, Vietnam. From 2012 to 2020, he served as a lecturer at Ho Chi Minh City University of Technology College, where he was actively involved in teaching and research. His research interests include artificial intelligence, numerical computation, optimization algorithms, and applied mathematics in computer science.
https://orcid.org/0000-0002-4035-1759

Nguyen Hong Son *received his B.Sc. in Computer Engineering from HCMC University of Technology in Ho Chi Minh City, and his M.Sc. and PhD in Communication Engineering from the Posts and Telecommunications Institute of Technology in Hanoi. His current research interests include communication engineering, information systems, AI/ML/DL, network security, and cloud computing.*
https://orcid.org/0009-0001-4466-7160

Huynh Trong Thua *is the Head of the Information Security Department, Faculty of Information Technology 2, at the Posts and Telecommunications Institute of Technology (PTIT), Vietnam. He earned his Bachelor's degree in Information Technology from Ho Chi Minh City University of Natural Sciences, his Master's degree in Computer Engineering from Kyung Hee University, Korea, and his Ph.D. in Computer Science from Ho Chi Minh City University of Technology, Vietnam National University. His research interests include cybersecurity, artificial intelligence, big data, and intelligent information systems. Dr. Huynh has published extensively in these areas and has made significant contributions to both academic and applied research communities.*
https://orcid.org/0000-0003-3934-1067

An International Journal of Optimization and Control: Theories & Applications
(https://accscience.com/journal/ijocta)